

Dependence of the Chiral Symmetry Restoration Transition on the Quark Self-Energy Kernel

A. Bender, W. Detmold and A.W. Thomas

Special Research Centre for the Subatomic Structure of Matter, and Department of Physics and Mathematical Physics, Adelaide University, 5005, Australia

Abstract

The dependence of the dressed quark propagator on the quark chemical potential is investigated in various models based on the Dyson-Schwinger equations. We find that the critical chemical potential of the chiral symmetry restoration transitions is strongly dependent on the nature of the interaction kernel in the infrared region.

The study of the thermodynamic phase structure of QCD has many implications for astrophysics and relativistic heavy ion collisions. An understanding of the behaviour of strongly interacting matter in regions of non-zero temperature and density will give insight into the nature of primordial baryogenesis and the dynamics of neutron stars. Heavy ion colliders such as RHIC and LHC will soon provide experimental data in thermodynamic regions where chiral symmetry is predicted to be restored.

The structure of QCD at non-zero temperature and zero density has been explored extensively using numerical simulations of lattice QCD. These results and other model based calculations suggest that there is a critical temperature, $T_{\text{crit}} \simeq 170\text{--}190$ MeV [1], above which normal nuclear matter undergoes a phase transition to a quark-gluon plasma in which chiral symmetry is restored. Unfortunately, current lattice simulation methods have significant difficulties when a non-zero quark or baryon density is introduced [2]. For this reason, studies in models that implement the pertinent features of QCD are important. Here, we present results from such a study utilising the Dyson-Schwinger equation (DSE) framework [3].

At present we make no attempt to incorporate the colour superconducting ground state that has been shown to occur at asymptotic quark densities [4]. The relevance of these results to QCD at densities of interest in nuclear physics (where perturbative results are suspect) is not well understood. These densities have only been investigated in simple approximations such as the Nambu–Jona-Lasinio model [5] and the Munczek-Nemirovsky (DSE) model [6] which may not be reliable representations of QCD in this regime. An extension of the current work may address these deficiencies and is under investigation.

In principle, the DSE's determine all possible information about a quantum field theory by providing all of its Schwinger functions. Unfortunately, they form a countably infinite set of coupled integral equations with the equation for an n -point Schwinger function depending

on $(n + 1)$ and higher point functions. Our approach is derived from these equations by specifying a scheme for truncating this infinite system through modelling the requisite, undetermined Schwinger functions.

Previously, simple DSE models [7,6] have been used to investigate the restoration of chiral symmetry as the quark density (or chemical potential) increases. A phase transition has been found at a critical chemical potential, $\mu_{\text{crit}} \sim 300\text{--}400$ MeV. Here we examine the effect on this result of using different quark self-energy kernels.

In Euclidean space (with metric $g^{\mu\nu} = \delta^{\mu\nu}$, and Clifford algebra $\{\gamma_\mu, \gamma_\nu\} = 2\delta_{\mu\nu}$, $\gamma_5 = -\gamma_1\gamma_2\gamma_3\gamma_4$), we separate the inverse quark propagator, S , at non-zero quark chemical potential, μ , into its spacelike and timelike vector parts, A and C , and scalar part, B :

$$S^{-1}(\tilde{p}; \zeta) \doteq i\vec{\gamma} \cdot \vec{\mathbf{p}}A(\tilde{p}; \zeta) + i\gamma_4\omega_p C(\tilde{p}; \zeta) + B(\tilde{p}; \zeta) \quad (1)$$

where the quark momentum $\tilde{p} \equiv (\vec{\mathbf{p}}, \omega_p = p_4 + i\mu)$. The propagator is renormalised at the (O(4) invariant) scale ζ which is large enough that

$$S^{-1}(\tilde{p}; \zeta)\Big|_{\tilde{p}^2=\zeta^2}^{\mu=0} = S_0^{-1}(\tilde{p}; \zeta) = i\gamma \cdot p + m_R(\zeta), \quad (2)$$

where S_0 is the free propagator for a quark with running current mass $m_R(\zeta)$. In terms of the regularised self-energy $\Sigma'(\tilde{p}, \Lambda)$, the inverse propagator can be expressed as

$$S^{-1}(\tilde{p}; \zeta) = Z_2^A i\vec{\gamma} \cdot \vec{\mathbf{p}} + Z_2(i\gamma_4\omega_p + m_{\text{bare}}(\Lambda)) + \Sigma'(\tilde{p}, \Lambda), \quad (3)$$

where $m_{\text{bare}}(\Lambda)$ is the bare, regularisation dependent mass occurring in the Lagrangian, Λ a regularisation parameter (we use $\int_k^\Lambda = \int_0^\Lambda \frac{k^3 dk}{(2\pi)^4} \int d\Omega_3$ with a simple cutoff regulator Λ), and Z_2^A and Z_2 are respectively, the spacelike and timelike field renormalisations, dependent on both the regularisation and renormalisation scales. As we renormalise at $\mu = 0$ where O(4) invariance is preserved, $Z_2^A = Z_2$.

The DSE satisfied by the self-energy is

$$\Sigma'(\tilde{p}, \Lambda) = g^2 \int_k^\Lambda D_{\mu\nu}^{ab}(p-k) t^a \gamma_\mu S(\tilde{k}) \Gamma_\nu^b(p, k), \quad (4)$$

where $D_{\mu\nu}^{ab}(q)$ and $\Gamma_\nu^b(p, k)$ are the full, nonperturbative gluon propagator and the quark gluon vertex respectively and $\{a, b\}$ are colour indices with $t^a = \frac{\lambda^a}{2}$ for the standard Gell-Mann SU(3) representation λ^a [3].

As is the case for the propagator, the self-energy can be expressed in terms of three scalar functions Σ'_A , Σ'_B and Σ'_C as

$$\Sigma'(\tilde{p}; \Lambda) = i\vec{\gamma} \cdot \vec{\mathbf{p}}\Sigma'_A(\tilde{p}; \Lambda) + i\gamma_4\omega_p\Sigma'_C(\tilde{p}; \Lambda) + \Sigma'_B(\tilde{p}; \Lambda). \quad (5)$$

These functions satisfy the coupled DSEs,

$$\Sigma'_X(\tilde{p}; \Lambda) = \int_k^\Lambda g^2 D_{\mu\nu}^{ab}(\tilde{p} - \tilde{k}) \frac{1}{4} \text{tr} \left[\mathcal{P}_X \gamma_\mu t^a S(\tilde{k}) \Gamma_\nu^b(\tilde{p}, \tilde{k}) \right], \quad (6)$$

where $X = A, B, C$; $\mathcal{P}_A = -(Z_1^A i\vec{\gamma} \cdot \vec{\mathbf{p}}/|\vec{\mathbf{p}}|^2)$, $\mathcal{P}_B = Z_1$, $\mathcal{P}_C = -(Z_1 i\gamma_4/\omega_p)$ and the trace is over Dirac and colour space. We constrain the vertex renormalisation Z_1 to be the same

as the field renormalisation, $Z_1 = Z_2$, which is consistent with the use of the bare vertex $\Gamma_\nu^b(\tilde{q}, \tilde{p}) = \gamma_\nu t^b$ [3].

The renormalisation condition (2) implies that

$$\begin{aligned} Z_2(\zeta^2, \Lambda^2) &= 1 - \Sigma'_A(\zeta, \Lambda)|_{\mu=0} \\ m_R(\zeta) &= Z_2(\zeta^2, \Lambda^2)m_{\text{bare}}(\Lambda) + \Sigma'_B(\zeta, \Lambda)|_{\mu=0}. \end{aligned} \quad (7)$$

Thus the regulator independent propagator functions are defined by

$$\begin{aligned} A(\tilde{p}; \zeta) &= 1 + \Sigma'_A(\tilde{p}; \Lambda) - \Sigma'_A(\tilde{p}; \Lambda)|_{\tilde{p}^2=\zeta^2}^{\mu=0} \\ B(\tilde{p}; \zeta) &= m_R(\zeta) + \Sigma'_B(\tilde{p}; \Lambda) - \Sigma'_B(\tilde{p}; \Lambda)|_{\tilde{p}^2=\zeta^2}^{\mu=0} \\ C(\tilde{p}; \zeta) &= 1 + \Sigma'_C(\tilde{p}; \Lambda) - \Sigma'_C(\tilde{p}; \Lambda)|_{\tilde{p}^2=\zeta^2}^{\mu=0}. \end{aligned} \quad (8)$$

Equations (1) through (8) form a coupled set of nonlinear integral equations for the quark propagator, and once the self-energy kernel $D\Gamma$ is specified we can proceed to solve them.

Here, we consider various models for this kernel, and in particular, separately for $D_{\mu\nu}^{ab}$ and Γ_μ^b . There are some constraints on the models that we can use to guide our choice; the main requirement is that they must be capable of producing dynamical chiral symmetry breaking (D χ SB) and confinement [8] as this is what is found experimentally. The behaviour of these objects in the ultraviolet region is also dictated by the results of perturbation theory.

The full Euclidean space gluon propagator can be written in Landau gauge as

$$g^2 D_{\mu\nu}^{ab}(q) = g^2 \delta^{ab} D_{\mu\nu}(q) = \delta^{ab} \left(\delta_{\mu\nu} - \frac{q_\mu q_\nu}{q^2} \right) \frac{\mathcal{G}(q^2)}{q^2}, \quad (9)$$

where we have assumed that the effect of quark chemical potential on the gluon propagator through quark loops is small in comparison to that on the quark propagator. To provide a model for it, we specify $\frac{\mathcal{G}(q^2)}{q^2}$. As the first example, we choose:

$$\frac{\mathcal{G}(q^2)}{q^2} = (2\pi)^4 \mathcal{G} \delta^4(q), \quad (10)$$

which corresponds to the Munczek-Nemirovsky [9] (MN) model. This model has been studied in the context of finite temperature and density [6,10] and has the advantage that the integral equations of the DSE reduce to algebraic equations (albeit nonlinear).

The remaining models are variations on the form:

$$\frac{\mathcal{G}(q^2)}{q^2} = 8\pi^4 \Delta \mathcal{G} \delta^4(q) + 4\pi^2 (2 - \Delta) \frac{\mathcal{G} q^2}{\omega^6} e^{-\frac{q^2}{\omega^2}} + \frac{4\pi^2 \gamma_m \left[1 - \exp\left(\frac{-q^2}{4m_t^2}\right) \right]}{q^2 \left(\frac{1}{2}\right) \ln \left[\tau + \left(1 + \frac{q^2}{\Lambda_{QCD}^2} \right)^2 \right]}, \quad (11)$$

where the one loop anomalous dimension $\gamma_m = \frac{12}{11N_c - 2N_f}$, the QCD scale parameter is set at $\Lambda_{QCD} = 0.275$ GeV, and $\tau = e^2 - 1$. The last term in Eq.(11) implements the results of perturbative QCD to one loop. However, the quantities we study in this paper are determined primarily by the low momentum structure of the kernel and are relatively insensitive

to this ultra-violet behaviour. The first two terms of the model provide some infrared enhancement to the self-energy, leading to dynamical chiral symmetry breaking (D χ SB). The exact form of the IR enhancement of the quark self-energy kernel is unknown [8]¹, and by varying Δ and to some extent ω it is possible to explore various possibilities. For $\Delta = 2$, the propagator (11) essentially reduces to that considered in Refs. [7,13], however we have also included the UV tail which provides the correct leading-log asymptotic behaviour for the quark propagator. For $\Delta = 1$ this is the propagator considered at zero density in Ref. [14]. Finally, with $\Delta = 0$ we get the propagator used in Ref. [15].

In order to motivate the different models used here for the vertex, we first briefly outline the method used to obtain the critical chemical potential. For a given self-energy kernel, the DSE's for the quark propagator are solved self-consistently to find solutions representing the Nambu-Goldstone phase (characterised by D χ SB) and a Wigner-Weyl phase (corresponding to the quark-gluon plasma where chiral symmetry is restored). The energetic stability of these two solutions is then compared using an effective action for the composite operators S and D .

One commonly used truncation of the DSE (6), called the rainbow approximation, involves replacing the full vertex in Eq. (6) by the bare vertex,

$$\Gamma_\nu^a(k, p) = t_a \gamma_\nu. \quad (12)$$

In this case, the correct action to use is the Cornwall-Jackiw-Tomboulis (CJT) effective action [16] which is given by

$$\mathcal{A}_{\text{CJT}}[S] = \text{TrLn} [S_0^{-1}S] + \frac{1}{2}\text{Tr} [\Sigma S]. \quad (13)$$

We wish to explore the effects of moving beyond the rainbow approximation (ideally to a vertex that respects the various symmetries of the full vertex, see Refs. [3,17]), but must first address the question of which effective action should be used to measure the energy of the different solutions. For a more complicated vertex, functionally dependent on the quark propagator, the CJT action is not the correct object to use [18]. However the correction required is so far only calculable in a limited number of cases². This restricts the types of models that we can use for the vertex.

Consequently, we use the next level of truncation of the DSE (6); a one loop vertex involving the non-perturbative quark and gluon propagators. This vertex was introduced in Ref. [19] and used further in Refs. [6,20]. In combination with the appropriate Bethe-Salpeter kernel, it preserves the axial-vector Ward identity and is systematically improvable. The form for this vertex is

¹Indeed, recent lattice calculations [11] and DSE studies [12] suggest the enhancement may in fact not occur in the gluon propagator but through the vertex. In our approach, it is full kernel $D\Gamma$ that is modelled and the particular separation into gluon propagator and vertex function is arbitrary.

²This is essentially the same problem that frustrates a consistent truncation of the DSE and corresponding BSE equations

$$\Gamma_{\mu;a}^{1L}(k,p) = t^a \left[\gamma_\mu + \frac{1}{6} \int_l^\Lambda g^2 D_{\rho\sigma}((p-l)^2) \gamma_\rho S(l+k-p) \gamma_\mu S(l) \gamma_\sigma \right]. \quad (14)$$

The correct action to use in combination with this vertex is,

$$\mathcal{A}_{\text{IL}}[S, D] = \mathcal{A}_{\text{CJT}}[S] + \mathcal{A}_\Gamma[S, D], \quad (15)$$

where [18],

$$\mathcal{A}_\Gamma[S, D] = -\frac{1}{24} \int d^4p d^4q d^4r D_{\rho\sigma}(p-q) D_{\mu\nu}(r-q) \text{Tr} [\gamma^\mu S_p \gamma^\rho S_q \gamma^\nu S_r \gamma^\sigma S_{p-q+r}]. \quad (16)$$

Having described the basis of the calculations, we now turn to the most important results. For the MN model with a bare vertex the analytic solutions are known. In the chiral limit, the two relevant solutions are:

$$\begin{aligned} S_1 : \quad & B(\tilde{p}) = 0 \quad A(\tilde{p}) = \frac{1}{2} \left[1 + \sqrt{1 + \frac{8\mathcal{G}}{\tilde{p}^2}} \right] \\ S_2 : \quad & B(\tilde{p}) = 2\sqrt{\mathcal{G} - \tilde{p}^2} \quad A(\tilde{p}) = 2. \end{aligned} \quad (17)$$

In order to define the symmetric and $D\chi\text{SB}$ solutions for the MN model at non-zero quark chemical potential, it is necessary to provide a prescription for the transition from solution S_2 to solution S_1 as $|\tilde{p}| \rightarrow \infty$. To generalise the $\mu = 0$ case (where the reality of B determines the transition point), we set $S_{D\chi\text{SB}} = S_2$ for $\Re(\tilde{p}^2) < G + \mu^2$ and $S_{D\chi\text{SB}} = S_1$ otherwise. We stress that while this prescription is a reasonable generalisation of the model to finite μ , it is essentially arbitrary and different results are obtained with other prescriptions [18].

For this model, the critical chemical potential (μ_{crit} such that $\Delta_{\text{CJT}} \equiv \mathcal{A}_{\text{CJT}}[S_{D\chi\text{SB}}] - \mathcal{A}_{\text{CJT}}[S_{\text{Symm.}}] = 0$) is displayed as a function of the coupling strength \mathcal{G} in Fig. 1. As \mathcal{G} is increased, there is a corresponding monotonic increase in μ_{crit} which can be fit exceedingly well with the simple form, $\mu_{\text{crit}}(\mathcal{G}) = 0.335\sqrt{\mathcal{G}}$. The ‘‘physical’’ value of the model parameter \mathcal{G} can be set by requiring that it yield the correct zero density pion decay constant, f_π . For this coupling, the critical chemical potential is $\mu_{\text{crit}} = 340$ MeV.

For the more phenomenologically appropriate models using the Maris-Roberts type effective quark-antiquark interactions, Eq. (11), the integral equations (6) are solved using an iterative procedure for $\zeta = 19$ GeV and $\Lambda \sim 10^3$ GeV. The quark condensate is extracted from the asymptotic behaviour of the quark mass function $M(p^2) = B(p^2; \zeta)/A(p^2; \zeta)$,

$$M(p^2) \xrightarrow{p^2 \rightarrow \infty} \frac{2\pi\gamma_m}{N_c} \frac{-\langle \bar{\psi}\psi \rangle^0}{p^2 \left[\frac{1}{2} \ln \left(\frac{p^2}{\Lambda_{\text{QCD}}^2} \right) \right]^{1-\gamma_m}}, \quad (18)$$

which is accurate up to $\mathcal{O}(\frac{\Lambda_{\text{QCD}}^2}{\zeta^2})$. The zero density pion mass and decay constant are calculated using analytic approximations to the solutions of the corresponding Bethe-Salpeter equation [13]. These values are used to fix the bare quark mass and the parameters \mathcal{G} and ω in the gluon propagator.

Calculations of the critical chemical potential in these models give qualitatively similar results to those of the MN model. Data from the $\Delta = 1$ and $\Delta = 2$ cases is shown for a range of \mathcal{G} in the upper panel of Figure 1. It is interesting to explore the parameter

dependence of these models. Figures 2 and 3 present the normalised CJT action differences $-\Delta_{\text{CJT}}[\mu]/\Delta_{\text{CJT}}[0]$ as a function of μ for variation of the three parameters \mathcal{G} , Δ and ω . The results for different parameter choices are normalised to -1 at zero chemical potential as $|\Delta_{\text{CJT}}[0]|$ increases rapidly with \mathcal{G} . For $\Delta = 2$, Fig. 2 shows that as the total infrared strength \mathcal{G} is increased μ_{crit} increases in a manner similar to that of the MN model. Fig. 3 shows the normalised action differences for variation with Δ (left panel, $\mathcal{G} = 0.26 \text{ GeV}^2$, $\omega = 0.3 \text{ GeV}$) and ω (right panel, $\mathcal{G} = 0.26 \text{ GeV}^2$, $\Delta = 1$). As Δ decreases from 2 (where the entire infrared strength is in the delta function at zero momentum) to 0 (where the effective quark-antiquark interaction vanishes at zero momentum), the critical chemical potential decreases for a given coupling strength and fixed value of ω . Similarly, as the infrared strength of the propagator is broadened by increasing ω for a given \mathcal{G} and Δ , μ_{crit} again decreases. Table 1 summarises the parameters used and the corresponding values of the critical chemical potential for the various models considered here.

The effect on μ_{crit} of using the one loop vertex is twofold. First, the solutions themselves are modified, resulting in a change to both the physical values for the model parameters and the action differences. Using the corrected action, $\mathcal{A}_{1\text{L}}$, and the MN gluon propagator, the critical chemical potential is $\mu_{\text{crit}}^{1\text{L}}(\mathcal{G}) = 0.279\sqrt{\mathcal{G}}$. Secondly, the correction to the action produces an additional shift. We illustrate this for the MN model though similar, (but less clean) conclusions can be drawn from the Maris-Roberts type models [18]. Figure 1 (dashed line) shows the curve of critical chemical potential for the one loop vertex MN model evaluated with the full action, $\mathcal{A}_{1\text{L}}$. Also illustrated in the bottom panel of this figure is the effect of the correction term, \mathcal{A}_{Γ} , on the critical chemical potential. Data are shown for the difference between the critical chemical potentials obtained from the one loop vertex solutions using the CJT and full, one loop actions; specifically for $\delta\mu_{\text{crit}} = [\mu_{\text{crit}}^{\text{CJT}} - \mu_{\text{crit}}^{1\text{L}}]/\mu_{\text{crit}}^{1\text{L}}$. It can be seen that the effect of the correction term is insignificant ($|\delta\mu_{\text{crit}}| < 2\%$ for the range of values for \mathcal{G} considered here) in comparison to the modification of μ_{crit} because of the use of one loop solutions.

In summary, the studies performed here make it clear that the critical chemical potential is an ‘‘observable’’ that is sensitive to the non-perturbative structure of the quark self energy kernel. For reasonable models with parameters fitted to the quark condensate, pion mass and decay constant, we find that μ_{crit} lies between 300 and 650 MeV. Our studies utilising a one loop vertex support the possibility that the CJT action, although not strictly appropriate, provides a reliable extraction of μ_{crit} for vertices other than the bare vertex. Whether this remains true for (physically) more acceptable vertices such as those of Ball and Chiu or Curtis and Pennington [17] remains an open question.

ACKNOWLEDGEMENT

This work was supported by the Australian Research Council and Adelaide University. We acknowledge helpful discussions with Reinhard Alkofer, Peter Tandy and Craig Roberts.

REFERENCES

- [1] For a review, see F. Karsch, Nucl. Phys. Proc. Suppl. **83**, 14 (2000).
- [2] I. M. Barbour, S. E. Morrison, E. G. Klepfish, J. B. Kogut and M. Lombardo, Nucl. Phys. Proc. Suppl. **60A**, 220 (1998).
- [3] For a recent review with emphasis on QCD thermodynamics, see C. D. Roberts and S. M. Schmidt, Prog. Part. Nucl. Phys. **45S1**, 1 (2000) [nucl-th/0005064]; Other useful reviews include R. Alkofer and L. von Smekal, hep-ph/0007355. and C. D. Roberts and A. G. Williams, Prog. Part. Nucl. Phys. **33**, 477 (1994).
- [4] K. Rajagopal and F. Wilczek, hep-ph/0011333; M. Alford, hep-ph/0102047.
- [5] M. Alford, K. Rajagopal and F. Wilczek, Phys. Lett. **B422** (1998) 247 [hep-ph/9711395].
- [6] J. C. Bloch, C. D. Roberts and S. M. Schmidt, Phys. Rev. **C60**, 065208 (1999).
- [7] A. Bender, G. I. Poulis, C. D. Roberts, S. M. Schmidt and A. W. Thomas, Phys. Lett. **B431**, 263 (1998).
- [8] F. T. Hawes, P. Maris and C. D. Roberts, Phys. Lett. B **440**, 353 (1998)
- [9] H. J. Munczek and A. M. Nemirovsky, Phys. Rev. **D28**, 181 (1983).
- [10] D. Blaschke, C. D. Roberts and S. M. Schmidt, Phys. Lett. **B425**, 232 (1998).
- [11] F. D. Bonnet, P. O. Bowman, D. B. Leinweber and A. G. Williams, Phys. Rev. D **62**, 051501 (2000)
- [12] P. Watson and R. Alkofer, hep-ph/0102332; R. Alkofer and L. von Smekal, hep-ph/0007355; D. Atkinson and J. C. Bloch, Mod. Phys. Lett. A **13**, 1055 (1998). L. von Smekal, R. Alkofer and A. Hauck, Phys. Rev. Lett. **79**, 3591 (1997);
- [13] M. R. Frank and C. D. Roberts, Phys. Rev. **C53**, 390 (1996).
- [14] P. Maris and C. D. Roberts, Phys. Rev. **C56**, 3369 (1997).
- [15] P. Maris and P. C. Tandy, Phys. Rev. **C60**, 055214 (1999).
- [16] J. M. Cornwall, R. Jackiw and E. Tomboulis, Phys. Rev. **D10**, 2428 (1974).
- [17] J. S. Ball and T. Chiu, Phys. Rev. **D22**, 2542 (1980); Phys. Rev. **D22**, 2550 (1980); D. C. Curtis and M. R. Pennington, Phys. Rev. **D42**, 4165 (1990).
- [18] A. Bender, W. Detmold, A. W. Thomas, *in preparation*.
- [19] A. Bender, C. D. Roberts and L. von Smekal, Phys. Lett. **B380**, 7 (1996).
- [20] G. Hellstern, R. Alkofer and H. Reinhardt, Nucl. Phys. **A625**, 697 (1997).

TABLES

Model	\mathcal{G} [GeV ²]	ω [GeV]	m_q [MeV]	$(-\langle\bar{q}q\rangle)^{1/3}$ [GeV]	f_π [MeV]	m_π [MeV]	μ_{crit} [MeV]
MN(bare)	1.0	-	17	0.216	93	138	340
MN(bare)	1.20	-	17	0.236	102	145	370
MN(loop)	0.93	-	15	0.211	93	137	270
MN(loop)	1.15	-	15	0.236	105	144	300
MR($\Delta = 2$)	0.82	-	9.8	0.236	90	138	630
MR($\Delta = 1$)	0.61	0.3	6.6	0.236	77	138	610
MR($\Delta = 0$)	0.45	0.3	5.7	0.236	75	139	530

TABLE I. Parameters and observables are shown for a variety of models studied. The quark masses, m_q , listed for the Munczek-Nemirovsky (MN) models are the bare masses as this model is not renormalised. For the Maris-Roberts (MR) type models the value listed is the renormalised mass at 19 GeV². The different cases for each particular model are when either the condensate or pion decay constant is fitted.

FIGURES

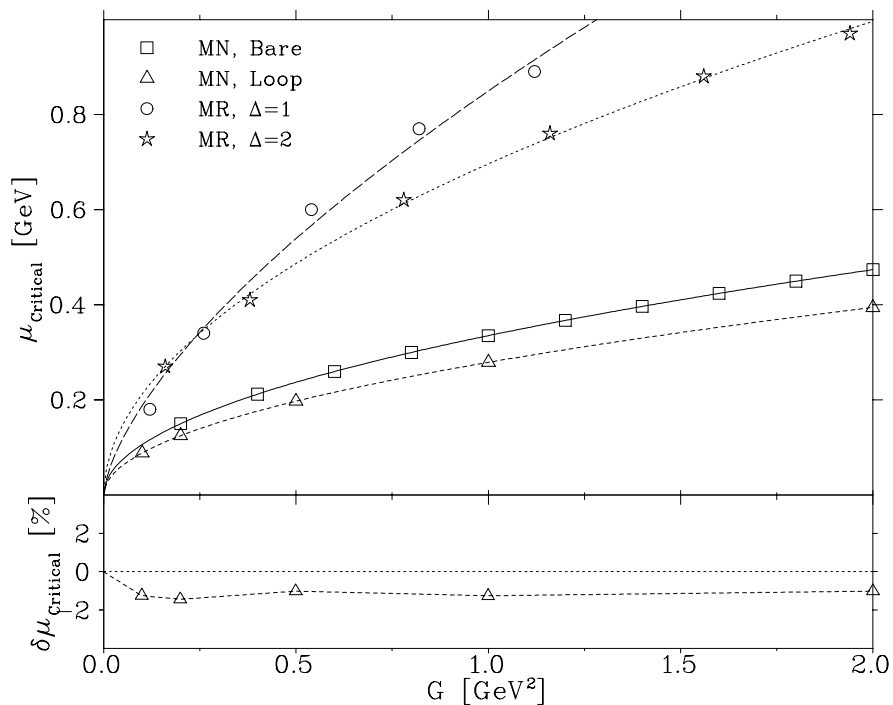


FIG. 1. In the upper panel, the calculated critical chemical potential is shown for the various self-energy kernels as a function of the coupling strength, \mathcal{G} (G in axes labels). The cases are: (open squares) Munczek-Nemirovsky gluon propagator and bare vertex (CJT action); (open triangles) MN gluon and one-loop vertex (calculated using one-loop action); (open circles) Maris-Roberts (MR) type propagator, bare vertex with $\Delta = 1$ and $\omega = 0.3$ GeV; (open stars) MR propagator, bare vertex with $\Delta = 2$. Simple fits of the form $\mu_{\text{crit}}(\mathcal{G}) = \alpha \mathcal{G}^\beta$ are shown for each data set. In the MN cases, the best fits occur with $\beta = 1/2$ and with $\alpha = 0.335(0.279)$ for the bare (loop) vertex. With the MR propagator the best fits are: ($\Delta = 2$ case) $\alpha = 0.696$, $\beta = 0.516$ and ($\Delta = 1$ case) $\alpha = 0.849$, $\beta = 0.656$. In the lower panel, the effect on the critical chemical potential of using the corrected action for the one loop MN model solutions is shown. This effect is small and the magnitude of $\delta \mu_{\text{crit}} = [\mu_{\text{crit}}^{\text{CJT}} - \mu_{\text{crit}}^{\text{1L}}]/\mu_{\text{crit}}^{\text{1L}}$ is less than 2 % over the range of \mathcal{G} studied.

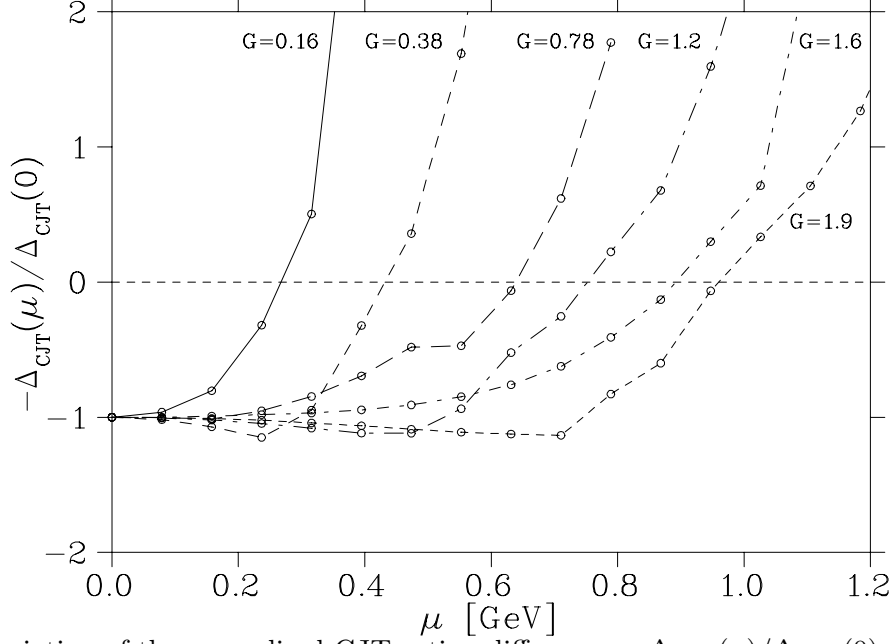


FIG. 2. Variation of the normalised CJT action difference, $-\Delta_{\text{CJT}}(\mu)/\Delta_{\text{CJT}}(0)$, with chemical potential is shown for a range of \mathcal{G} (labelled in units of GeV^2). The critical chemical potential for a given \mathcal{G} is reached at the zero intercept of that curve.

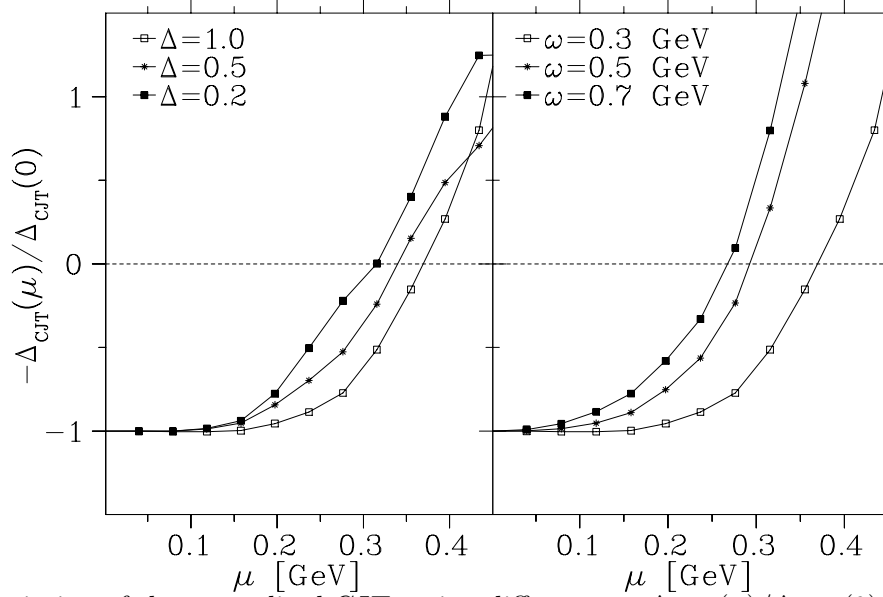


FIG. 3. Variation of the normalised CJT action difference, $-\Delta_{\text{CJT}}(\mu)/\Delta_{\text{CJT}}(0)$, with chemical potential is shown for a range of Δ (left panel, with fixed $\mathcal{G} = 0.26 \text{ GeV}^2$ and $\omega = 0.3 \text{ GeV}$) and ω (right panel, with $\Delta = 1$ and fixed $\mathcal{G} = 0.26 \text{ GeV}^2$).